MAJIS VIS-NIR channel: Performances of the Focal Plane Unit - Flight Model

Paolo Haffoud[a], Antoine Arondel[a], David Bolsée[b], Vincent Carlier[a], John Carter[a], Miriam Cisneros-González[b], Jean-Pierre Dubois[a], Cydalise Dumesnil[a], Gianrico Filacchione[c], Ludovic Gonnod[a], Cyrille Hannou[a], Véronique Hervier[a], Özgür Karatekin[b], Christian Ketchazo[a], Yves Langevin[a], Jean-Christophe Le Clec'h[a], Benoit Lecomte[a], Gilles Morinaud[a], Nuno Pereira[b], Giuseppe Piccioni[a], Ann-Carine Vandaele[b], Lionel Van Laeken[b], Mathieu Vincendon[a], Francois Poulet[a], and the MAJIS team.

[a]Institut d'Astrophysique Spatiale (France), Rue Jean Dominique Cassini, 91440 Bures-sur-Yvette, France ; [b]Royal Belgian Institute for Space Aeronomy, Av. Circulaire 3, 1180 Uccle, Belgium; [c]INAF - Istituto di Astrofisica e Planetologia Spaziali, Via Fosso del Cavaliere 100, 00133 Rome, Italy.

ABSTRACT

The JUICE (JUpiter ICy moons Explorer) mission by ESA aims to explore the emergence of habitable worlds around gas giants and the Jupiter system as an archetype of gas giants. MAJIS (Moons and Jupiter Imaging Spectrometer) is the visible to near-infrared imaging spectrometer onboard JUICE which will characterize the surfaces and exospheres of the icy moons and perform monitoring of the Jupiter atmosphere. The launch is scheduled for 2023 with the first MAJIS observations inside the Jovian system occurring more than 8 years later.

The MAJIS optical head is equipped with two Teledyne H1RG detectors, one for each of the two spectrometer channels (VIS-NIR and IR). This paper describes the characterization of the VIS-NIR Focal Plane Unit. These detectors will be operated in a non-standard way, allowing near/full-frame retrieval over short integration times (<< 1 sec) while maintaining good noise performance.

After a quick description of the characterization strategy that was designed to evaluate the performances of the VIS-NIR detector according to the MAJIS operational specifications, the paper will address the data analyses and the main results of the characterization campaign. The major performance parameters such as dark current, linearity, noise, quantum efficiency, and operability will be presented and compared with the requirements.

Keywords: JUICE, MAJIS, visible and near-infrared, spectrometer, characterization, H1RG, detector

1. INTRODUCTION

1.1 Instrument description

The Moons And Jupiter Imaging Spectrometer (MAJIS) instrument is the visible to midwave IR (0.5 to 5.56 μm) spectral mapper on board the Jupiter Icy Moon Explorer (JUICE) scheduled to launch in 2023. The JUICE satellite will tour the Jovian system, performing close flybys of 3 of the Galilean Moons (Callisto, Ganymede and Europa) before entering its final orbit around Ganymede. The main scientific goals of JUICE are the investigation of the emergence of habitable worlds around gas giants and the study of Jupiter as an archetype of gas giants. MAJIS will mainly acquire hyperspectral cubes of data for exploring and mapping the surface composition of various units of scientific interest for the Galilean Moons. This include the study of Ganymede's ice-shell and surface features and the investigation into the chemistry of surface material and active processes present on Europa and Callisto.

The telescope optics focus light on a slit to form an image one-line high and approximately 400 columns wide. After the light passes through the slit, a dichroic filter will separate the light between two channels which will be ultimately collected by two detectors or Focal Plane Arrays (FPAs). Both detectors are H1RG detectors (responding to different spectral ranges) provided by Teledyne Cie. Due to the relatively high levels of irradiance of the targets compared to the detector well depths, and to mitigate the high rate of radiation spikes from the Jovian environment, these detectors will be operated in a nonstandard way, allowing near/full-frame retrieval over short integration times (<< 1 sec) while

maintaining good noise performance. This article presents the results of the characterization of the VISNIR detector. A companion article[1] presents the results of the characterization of the flight IR detector.

1.2 Focal Plane Unit (FPU)

The VIS-NIR focal plane unit (FPU) consists of several components. Some of the main components are the focal plane electronics (FPE) and a high band pass linear variable filter which is set in front of the FPA so as to exclude photons from high grating orders.
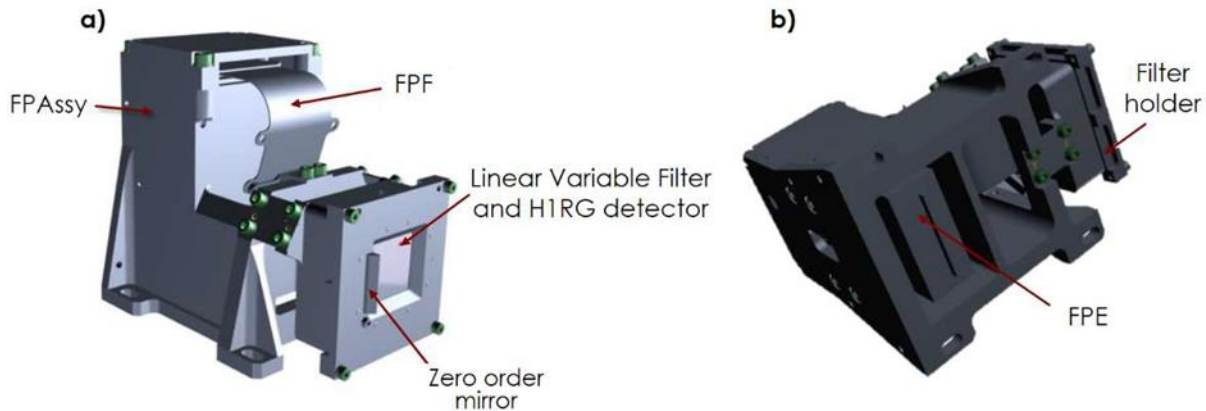

Figure 1. Views of the VIS-NIR FPU and its parts: a) frontal view, b) rear view

The key element of the FPU is the H1RG detector. The H1RG detectors are composed of 1024x1024 pixels with an 18 μm pitch. The 4 lines and columns on each edge of the FPA are not connected to the sensitive layer ("reference pixels"). Each of the 1024 lines (1024 pixels) is converted into digital data through 16 independent video channels sampling the data at two readout frequencies (100 kHz and 1 MHz[2]). The detector is therefore composed of 16 outputs of 1024x64 pixels.

In flight, these detectors will typically be binned two by two (nominal operating mode). Out of the 512x512 remaining 36 μm by 36 μm binned pixels, only 400x512 pixels will be illuminated and therefore read. The instrument will take slit spectral images, the first dimension 400 pixels will correspond to the position along the slit and the second 512 spectels (nominal, up to 640) will correspond to the wavelengths sampled by MAJIS.

2. CAMPAIGN DESCRIPTION

2.1 Objectives

The FPU (FPA+FPE) is a critical element of the instrument and its performances will have a major impact on the overall performances of MAJIS.

The aim of this campaign was to evaluate the performances of the FM VIS-NIR detector (FPA). The parameters used to assess the performances were the dark current, linearity, noise, quantum efficiency and operability.

2.2 Set-up

The VIS-NIR FPA characterization facility includes the following elements[3]:

- A vacuum chamber which houses the FPU

- An optical bench which provides the monochromatic beam

- A TGSE software to manage the thermal and vacuum control of the chamber[4]

- A security system to protect the detector in case of failure of the equipment

- An OGSE software to remotely control the optical equipment and detector

To perform the FM VIS-NIR detector campaign, the configuration described in the diagram shown in Figure 2. was used.
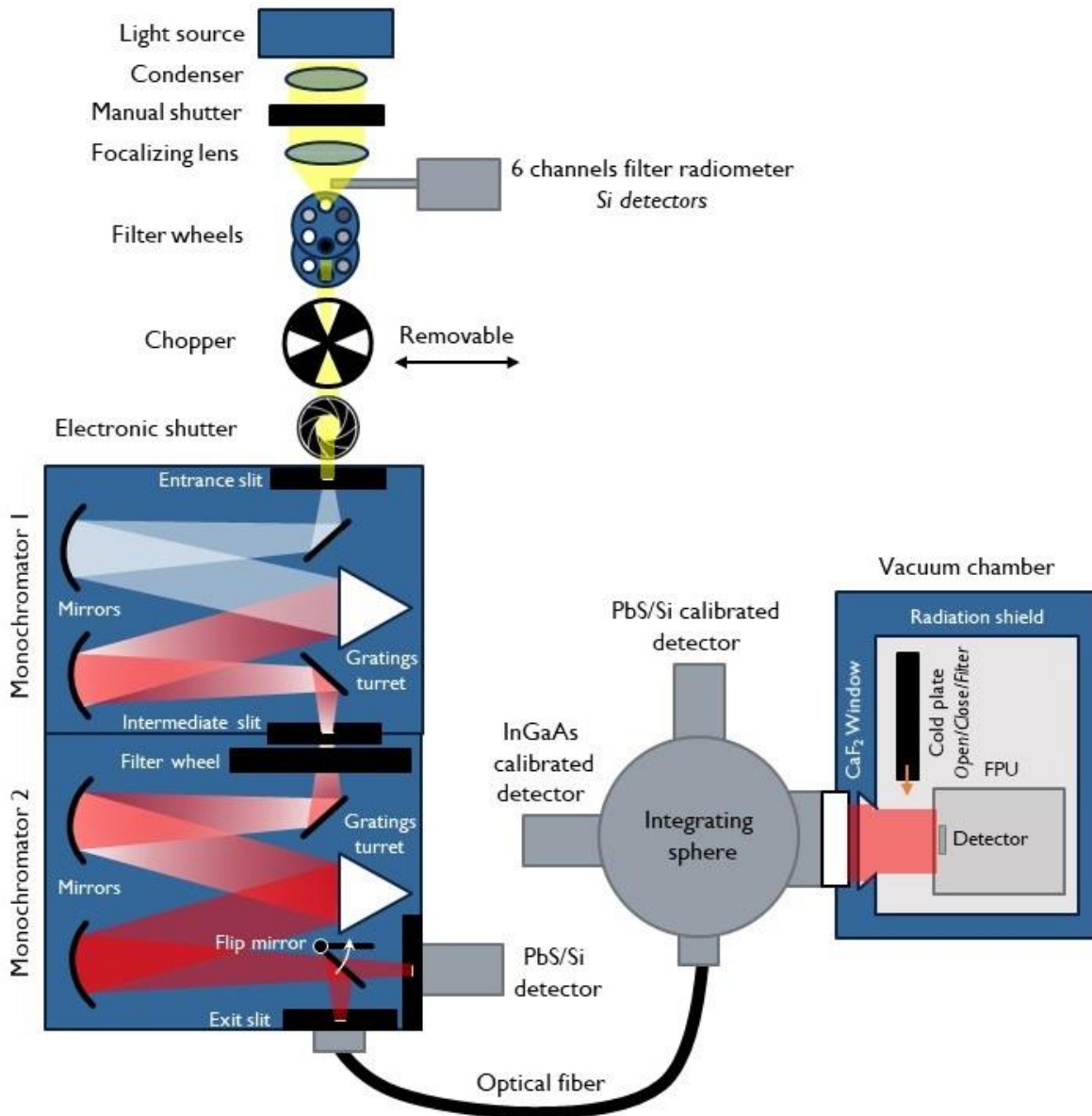

Figure 2. Optical diagram of the configuration 2 for the VIS-NIR calibration facility

In this configuration, a monochromator is coupled with a light source to provide a monochromatic beam that can be adjusted in wavelength (from 500 nm to 2550nm with an accuracy of 0.2 nm), full width at half maximum and output flux. The monochromatic beam is then guided through an optical fiber into an integrating sphere. The integrating sphere then feeds light onto the detector.

A motor can be used to move a cold plate, or 2 short-wave pass filters (SWPF2) stuck together in front of the FPA. This results in 3 possible configurations: closed (cold plate), SWPF2 (with the filters) or open (nothing in front of the FPA). The cold plate is used to reduce as much as possible the flux reaching the detector. The SWPF2 is used to reduce the thermal flux coming from the integrating sphere outside the chamber while letting monochromatic fluxes pass through for λ < 1400 nm. The open position is used when a monochromatic flux with λ > 1400 nm is necessary.

2.3 Tests description

Prior to the characterization a pre-campaign was held during three days. The results of this pre-campaign will not be fully detailed in this paper. These tests allowed:

● the tuning of the parameters and biases of the H1RG detector,

● an assessment of the stray light coming from the characterization setup in all configurations,

● a determination of the alignment of the setup,

● a verification of the behavior of the detector in non-nominal settings.

The main test campaign was focused on characterizing the detector through several performance parameters.

During the campaign, there were 4 main settings for the detector:

● Two acquisition speeds are available (100 kHz and 1MHz). **All tests were performed at both speeds.**

● **The number of frames per measurement was set at 32 for all tests**, to allow for a good statistic.

● The delta-integration time (DIT) depended on the goal of the test performed. The DIT of each frame could vary between 80 ms to 4000 ms using the 1 MHz mode and between 800 ms to 4800ms using the 100 kHz mode for full frame acquisition (1024x1024).

● Windowing makes it possible to select a given number of rows out of the 1024 H1RG rows. This was used when the test required a DIT below 80 ms for the 1 MHz and below 800 ms for the 100 kHz mode: The minimum DIT is proportionally reduced as the fraction of the total 1024 rows acquired. (e.g. using a 512-row window reduces the minimum DIT by half)

Additionally, there were 4 calibration setup parameters:

● **The FPA was set at 3 different temperatures for most tests, a few tests were only performed at nominal temperature.** These temperatures correspond to the nominal (132 K), minimum (125 K) and maximum (144 K) expected operating temperatures of the VIS-NIR detector in-flight.

● The wavelength of the monochromatic flux could be adjusted from 500 nm to 2550nm.

● As seen previously, three positions were available for the window of the vacuum chamber, open, closed by the cold-plate (for dark measurements), and filtered by the SWPF2.

● The incoming flux on the detector was adjusted depending on the needs. Notably, two consecutive filter wheels were available.

Nominally, each measurement would require a dark acquisition performed slightly before or after using the same detector settings (This is the operational procedure in-flight for optimized detector performances). Due to planning constraints these dark acquisitions were not systematically performed. This leads to apply a specific procedure to simulate a dark correction (see section 3), resulting in slightly underestimated performances.

The read-out conversion gain (in electrons per digital number, e-/DN), noise model, linearity and linear range were characterized using the same measurements. For the assessment of the linearity in integration time, acquisitions were performed with DITs varying between ¼ of the minimum full-frame DIT up to the maximum DIT. The wavelength and flux level were picked to allow for the most complete exploration of the full-well capacity (FWC).

The dark current (DC) was characterized with a similar approach to the linearity except the flux was reduced as much as possible using the cold-plate.

The read-out noise (RON) was characterized using the variance in signal for each pixel for 32 acquisitions with as little signal as possible. (i.e. minimum DIT and cold-plate in front of the FPA)

The quantum efficiency (QE) measurements were performed at several wavelengths ranging from 400 nm to 2550 nm. The flux and DIT were selected to remain well within the linear range while providing enough signal. Both the SWPF2 and the open position were used depending on the wavelength.

The operability is derived from a combination of criteria applying to previously mentioned performance parameters.

3. DATA REDUCTION

3.1 Data processing

All images acquired during this campaign were acquired using correlated double sampling or CDS (i.e. subtracting two successive acquisitions from one another so as to remove correlated offset perturbations). This type of measurement will also be the nominal operation in-flight.

A first step of post-processing which is required for characterization data is "row correction". A median average of the 4 "reference pixels" at the beginning and end of each row (therefore sum divided by 4) is subtracted from the 1016 active pixel values as representative of the expected level without signal.

The next step in the post-processing is "dark subtraction" which for the FPA FM VIS-NIR campaign corresponds to "background" subtractions (a frame obtained with a shutter closed and all sources off is subtracted from frames obtained with a source on). Background subtraction is very effective for mitigating the impact of ADC drift[2], which is specific to columns each 64 pixels wide. During in-flight operations, line correction and background subtraction will be performed by the VIS-NIR proximity electronics unit of MAJIS for nominal data acquisition, so that these steps will not be needed.

When dark frames were not available, an additional "column" correction was added to the post-processing. This correction consists in the subtraction of a "mean row" which is computed as the average of the 4 top reference rows (1020, 1021, 1022, 1023). While not equivalent to background subtraction, this correction is aimed at reducing the impact of the 16 output offsets. This procedure works quite well with 100 kHz readout and it provides a first approximation with 1 MHz readout[2].

Then, the DN signal is transformed into electrons by multiplication using the conversion gain.

However, a linear decrease of the conversion efficiency of the detector ("transimpedance", $\mu V/e-$) over the bottom half of the dynamic range was observed. On this basis, the signal has been first corrected for the transimpedance decrease so as to better match a linear behavior as follows:

$$\mathrm{DN_{cor}} = \mathrm{DN}\, \frac{1}{(1 - k \times DN)} \tag{1}$$

, where k is the transimpedance decrease parameter. The data reduction pipeline is summarized in the diagram below:
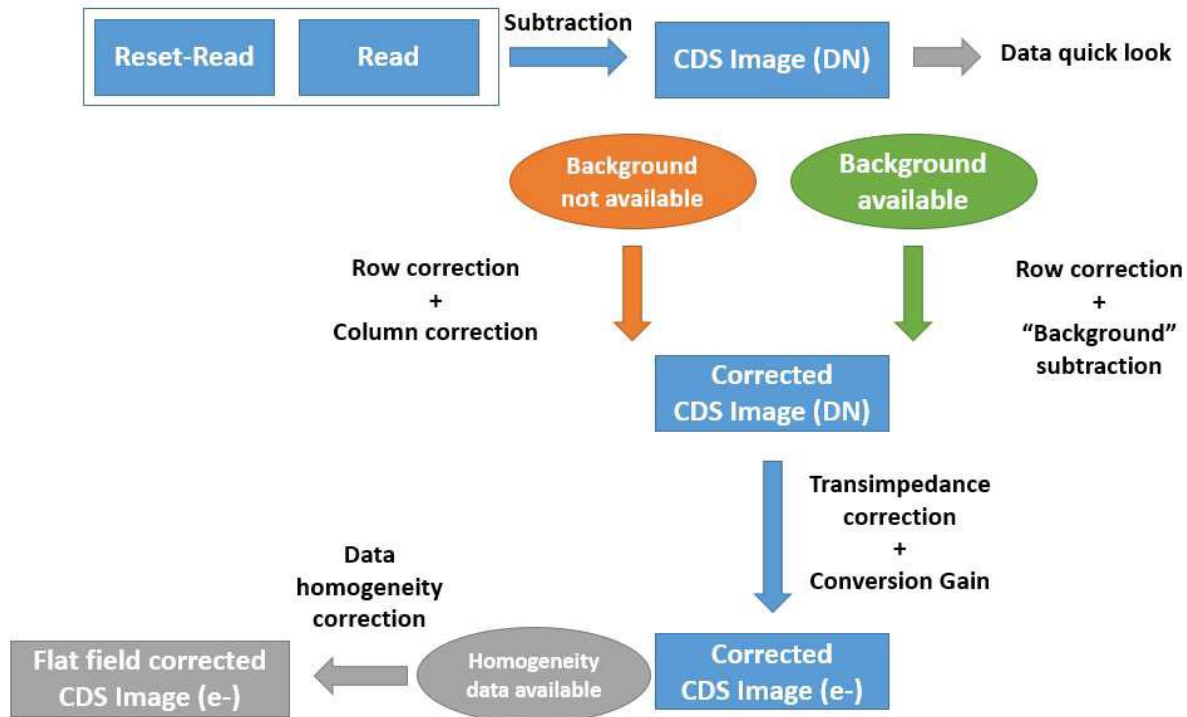
Figure 3. Data processing diagram – The nominal data processing is Background subtraction.

3.2 Definition of the performance parameters

Read-out gain and noise model

Once the linear decrease of the transimpedance is applied to both the signal and the noise (see previous section), a noise model as a function of signal level in DN provides a first estimate of the gain G in e-/DN, assuming an integration-time independent and constant contribution (readout noise + conversion noise) and a signal dependent stochastic contribution (shot noise):

$$\sigma \times G = \sqrt{\sigma_{fix}^2 \times G^2 + S_{DN} \times G} \tag{2}$$

where σ is the total noise, σ_{fix} the fix noise (corresponding in this case to the RON) and S_{DN} the signal in DN. Note that the RON depends on the acquisition mode.

The gain and noise model are characterized by comparing the median standard deviation of the pixels to the mean signal of the observation for a selection of pixels in a homogeneous area of the detector.

As this performance parameter is not expected to be temperature dependent, it has only been characterized at 132K.

Linearity (+ Linear range, Full-well Capacity)

The goal of this measurement is to assess the quality of the linear behavior and evaluate the full-well capacity and linear range to provide an estimation of the quantity of electrons that can be captured by the detector while remaining nominal.

The linearity measurements have been performed by keeping the flux constant while the DITs were increased.

The full-well capacity is estimated at saturation. Linearity measurements below 50% of full-well capacity are used to compute a least-square linear fit of the data versus DIT or flux. This linear fit also gives the 5% and -5% deviation to linearity lines.

The linear range can then be determined based on the intersection between the linearity data and one of the 5% deviation lines (-5% line in practice).

The deviation to linearity is also computed using the linear fit. (dev$_\%$=100$\times$(data-fit)/fit) The deviation to linearity can be used to assess the quality of the linear behavior and incidentally to validate the quality of the transimpedance decrease parameter. (The flatter the deviation to linearity the better the quality of the linearity.)

Dark currents

Due to a significant amount of stray light on the detector from the experimental setup with the cold-plate in front of the detector during this campaign, the dark currents could not be estimated on the entire 1024x1024 array.

During the following campaign, the stray light was reduced and the bottom rows of the detector were the least affected by the remaining stray light. Therefore, the estimation of the dark current for the detector will be based on the lower signals observed at the bottom of the FPA on these images.

Read-out Noise Map

The RON assesses the impact of a pixel's stochastic nature for low signals. For each pixel, it is estimated using the noise model (Eq. (2)), by taking the variance of a given pixel across all 32 acquisitions and subtracting the mean signal measured for this pixel.

The resulting map and distribution of RON is highly influenced by the number of images used to compute the standard deviation. The estimated variance affected to the RON can take negative values due to the error in the estimation of the total noise using the standard deviation over a small sample of acquisitions (32 images). The RON estimations are therefore not used as accurate measurements of the RON for a specific pixel, but to assess the behavior of the detector as a whole.

Quantum efficiency

This measurement aims at estimating the ratio between the electrons collected by a pixel to the photons it receives.

QE measurements have been performed at different wavelengths between 400 nm to 2550 nm. However, due to the limitations of the setup introduced by the bandpass of the SWPF2, two types of QE measurements have been performed:

●	(400 nm < λ < 1400 nm). The SWPF2 has been placed in front of the FPA and the 100kHz acquisition mode has been used. The monochromator's flux was adjusted to remain below saturation, but with enough signal to provide a good SNR.

●	(1400 nm < λ < 2550 nm). The "open" configuration and the 1MHz acquisition mode have been used in conjunction with 256 rows acquisitions to lower the minimum DIT to 20 ms and ensure that the thermal flux does not saturate the detector. Due to the very significant thermal flux and the low integration time, the monochromator's flux was set to its maximum (saturation was not reached) to maximize the SNR.

First before each QE measurement a background measurement (source OFF) has been performed, these background measurements were then subtracted to the QE images. The remaining electron signal from QE images have been normalized based on absolute radiometry measurements at the center of the detector. The incoming flux was not homogeneous, resulting in an overestimation of the variation of the QE across the FPA.

As this performance parameter is not expected to be temperature dependent, it has only been characterized at 132K.

Operability

The definition selected for the operability is as follows:

●	Read-out noise < 70 e-

●	Signal > 200 e-, for images where the median signal > 50% FWC (dead pixels excluded)

●	Signal < 200% median signal, for images where the median signal < 10% FWC (hot pixels excluded)

For each connected pixel of the detector, these 3 criteria will be tested. If one condition is not met, the pixel is considered inoperable. The total operability of the detector corresponds to the ratio of operable pixels to connected pixels.

4. RESULTS

4.1 Read-out gain and noise model

Figure 4. shows that the noise data acquired between fits very well for the noise model (see Eq. (2)).
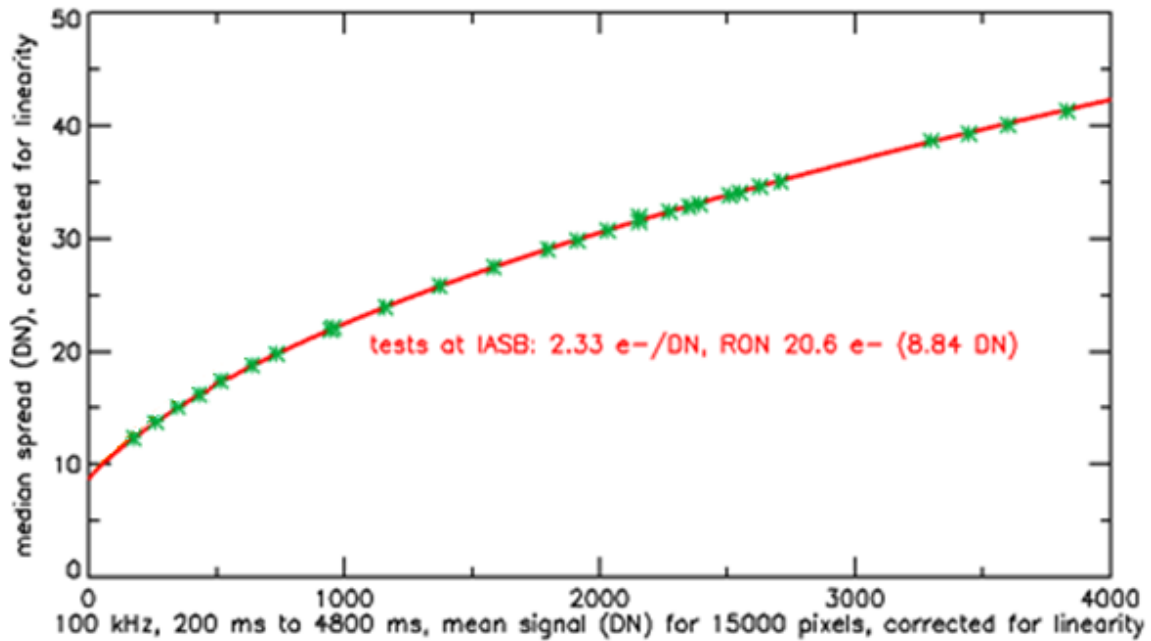

Figure 4. Noise (in corrected DN) as a function of signal (in corrected DN) for the detector at 132 K. In the 0 – 4000 DN signal range, the transimpedance follows very closely a linear decrease law. Applying Equation (2) with a gain of 2.33 e-/DN and a fixed noise ("RON") of 20.6 e- provides the best fit to the data over this signal range.

Additionally, for these H1RG detectors an "Inter Pixel Correlation" (IPC) effect has been previously described[5]. This can lead to an overestimation of the gain, resulting in quantum efficiencies higher than 1. To compensate, an IPC factor which was previously characterized to be 0.93 has to be applied to the gain estimation.

A previous characterization of the two readout modes showed that the 1 MHz readout provides DN values 15.54 times lower than the 100 kHz readout. Therefore, the 1 MHz read-out gain could be deduced from the 100 kHz results. Finally, the RON at 1 MHz was derived using the same procedure as for the 100 kHz. The results are summarized in Table 1.

Table 1. Gain/RON performances summary.

Acquisition mode	Read-out gain (e-/DN)	Read-out noise (e-)
(100 kHz)	2.16	19
(1 MHz)	33.56	34

4.2 Dark Currents

These measurements were performed during a follow-up campaign aimed at characterizing the FPU with the LVF in front of the detector.

Based on the observations made during the first campaign, a mitigation was taken to reduce the straylight reaching the detector inside the vacuum chamber afterwards allowing a more accurate characterization of the dark current.

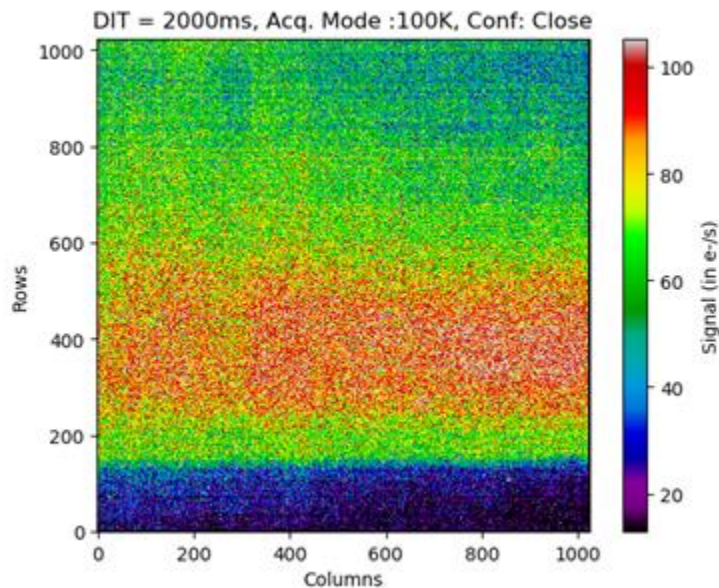The following figure (Figure 5.) shows an image captured at 132K in dark conditions.

Figure 5. Closed configuration background – 100kHz – 2000ms (Flux in e-/s) – FPU with LVF characterization campaign

The signal observed on Figure 5. has a significant dependency with the rows of the detector. Based on the signal levels being significantly higher than the expected dark currents for this type of detectors, it was deduced that this image is probably still impacted by residual straylight.

Using the signal levels from the bottom rows we can estimate that the dark currents are < 15 e-/s at 132K, which is closer to the expected values. Such dark currents will not have a significant impact on the SNR of the instrument during the mission.

4.3 Read-out Noise

The following RON maps are estimated across 32 images with as little flux as possible. The results of the measurements at 132 K are shown in Figure 6.
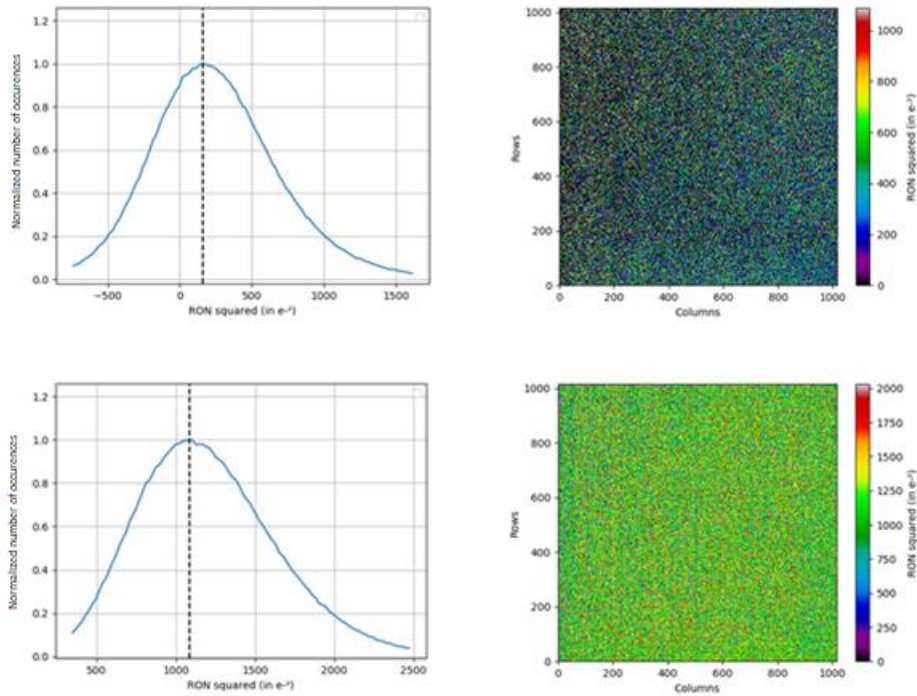
Figure 6. *Top left:* histogram of RON estimations for all pixels with the 100 kHz mode. *Top right:* mapping of RON estimations for all pixels with the 100 kHz mode. *Bottom left:* histogram of RON estimations for all pixels with the 1 MHz mode. *Bottom right:* mapping of RON estimations for all pixels with the 1 MHz mode. - Measurements performed at an FPA temperature of 132 K.

As mentioned in section III.B.4), the first histogram (see Figure 6. *Top left*) shows that for some pixels the estimated variance of the RON is negative because of an underestimation of the actual noise due to the stochastic nature of using a standard deviation across 32 images. Both maps (see Figure 6. *Top right* and *bottom right*) do not show a correlated pattern across the full FPA (any possible correlated pattern would be below the stochastic effect of the estimator). The distribution of the RON is centered around 13 e- (RON² ~ 160 e-²) for the 100 kHz mode and around 33 e- (RON² ~ 1100 e-²). For most pixels the 70 e- RON constraint for operability (which corresponds to 4900 in RON²) is still respected.

4.4 Linearity

The results of the linearity measurements with an FPA at 132K are shown in Figure 7. below.
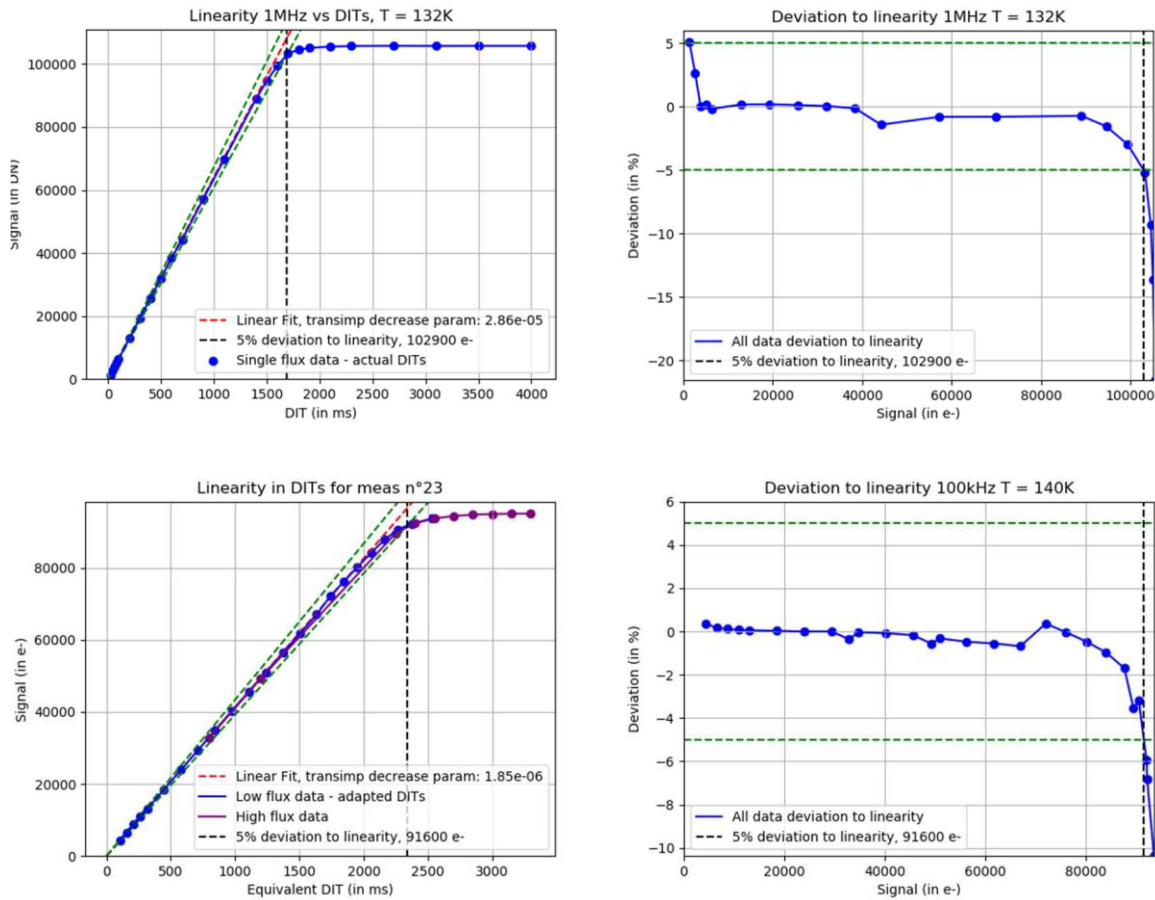
Figure 7. *Top left: Linearity vs DITs measurements for the 1 MHz mode. Top right: deviation to linearity measurements for the 1 MHz mode. A significant non-linearity can be seen on this figure for low flux. As explained in more details below, this is an effect of the post-processing and not the detector itself. Bottom left: Linearity vs DITs measurements for the 100 kHz mode. The flux initially used for the 100 kHz measurement were too low to reach the full saturation at 4800ms. Therefore, a second set of measurements was performed with higher fluxes to complete this measurement. Bottom right: deviation to linearity measurements for the 100 kHz mode*

The linearity of this H1RG detector remains within 2% of deviation to linearity for the large majority of its dynamic. It only displays non-linear behaviors for very low signals and close to saturation. The linear range and FWC both increase by more than 5% between the 100 kHz and the 1 MHz modes. (This holds true for all temperatures).
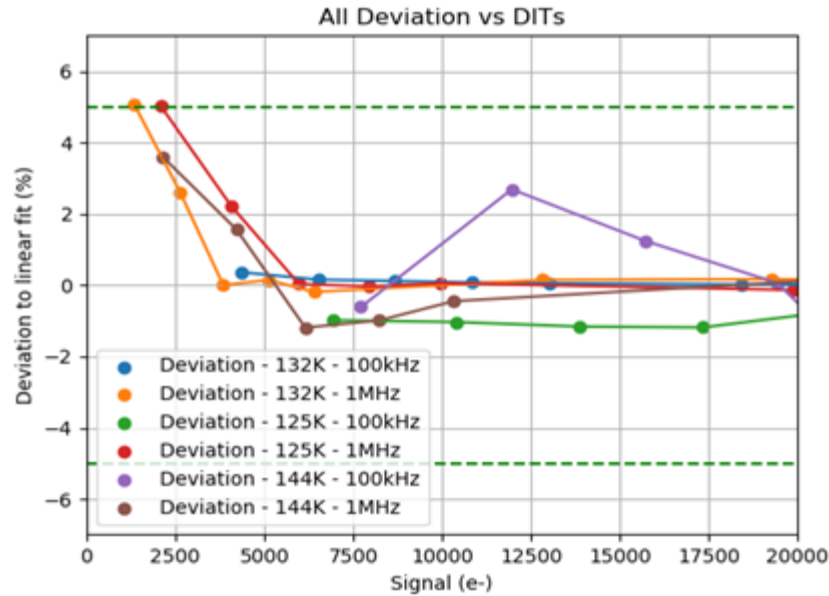
Figure 8. Median pixel deviation to linearity versus integration time (ms) for low flux - All Temperatures

For low signal, we investigated more closely the possible origin of this non-nominal behavior. As shown in the previous figure (Fig. 8), it occurs at all temperatures. The deviation remains small for signals > 5000 e-, and the most significant deviation is observed for the lowest signals. For very low signals, the deviation starts at a value >5%. This deviation decreases linearly to ~0% around 5000 e-. Tests performed with different setups and detectors show that this deviation is most likely a result of the column correction applied due to the absence of dark frames for linearity measurements. In-flight, the dark subtraction will remove this non-nominal behavior.

The full linearity test results are summarized in Table 2.:

Table 2. Gain/RON performances summary.

Temperature (K)	Acquisition mode	Linear range (5%) (e-)	FWC (e-)
125	100kHz	95,300	99,000
132	100kHz	91,600	95,000
144	100kHz	81,900	87,000
125	1MHz	101,100	105,000
132	1MHz	102,900	107,000
144	1MHz	95,900	100,000

4.5 Quantum Efficiency

The following QE measurements were performed in the open configuration, with all the thermal background reaching the FPA, therefore the subtracted background had a much higher magnitude compared to the backgrounds using the SWPF2. This led to the SNR being lower for these QE measurements.

To derive the QE from these measurements, both a homogeneity correction of the illumination and the absolute radiometry measurements are required. Unfortunately, the homogeneity data was lacking and this correction not performed, which can partly explain the spatial variation observed over the surface of the detector.
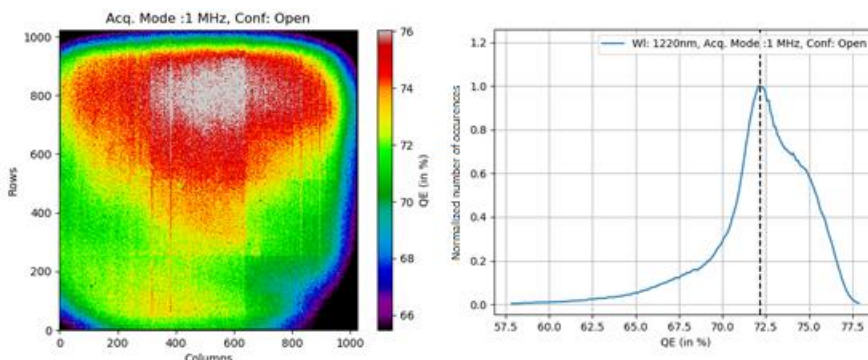

Figure 9. QE - 1 MHz - 1220nm - No flat field correction - *Left:* mapping of the QE measurements across the detector. Artefacts remain in the x-axis direction due to the post-processing (no dark subtraction), and in the y-direction due to the windowing used and the DITs selected being very close to minimum. *Right:* normalized histogram of QE measurements.

It also impacts the accrruacy of the measurements of the absolute radiometry. Therefore, all QE measurements have a relatively large uncertainty. But overall, the retrieved values are n agreement with the expectations for such detector.

Table 3. QE performances summary.

Lambda (nm)	Configuration	Acquisition mode	Peak QE (%) (no homogeneity)	N° pixels <35%
1220	Open	1 MHz	72	222
1500	Open	1 MHz	78	225
1750	Open	1 MHz	80	222
2000	Open	1 MHz	82	216
2250	Open	1 MHz	86	218
2450	Open	1 MHz	92	212
2500	Open	1 MHz	87	214

4.6 Operability

The measurements required for the operability characterization were available only for FPA temperatures of 125 K and 132 K. The results of the operability analysis are summarized in the table below:

Table 4. Operability performances summary.

Temperature (K)	Acquisition mode	N° Dead pixels	N° Hot pixels	N° high RON pixels	N° of non-operable pixels	Operability (%)
125	100kHz	67	2357	1358	3,476	99.66
125	1MHz	32	2386	446	2,664	99.74
132	100kHz	67	2545	858	3,156	99.69
132	1MHz	32	2428	730	2,929	99.72

The non-operable pixels are dominated by the hot pixels. The results do not show a significant dependency of the operability with the FPA temperature for these two temperatures.

In terms of operability, the VIS-NIR FM detector is performing much better than the constraints, with at most 0.34% of inoperable pixels while the objective was less than 5%.

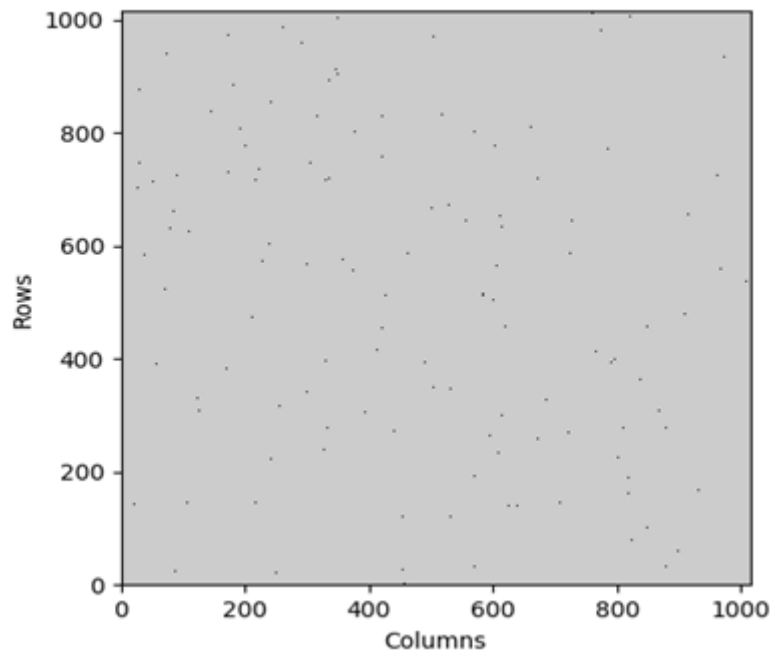The figure below shows a map of the non-operable pixels (in black) at 132 K using the 1 MHz mode:

Figure 10. Operability map - 1 MHz - 132 K

5. SUMMARY OF PERFORMANCES

The following table presents a summary of the performances at 18-μm pixels. The performances at the optical MAJIS pixels (36x36 μm²) are in the table below.

Table 5. Summary of 18-μm pixels FPA performances.

Performance parameter	Requirements	Measured (125K)	Measured (132K)	Measured (144K)
RON (100kHz) **(e-) (1MHz)**	<20 <40		19.5 34	
GAIN (100kHz) **(e-/DN) (1MHz)**			2.16 33.56	
DARK (e-/s)	<2,500		<15	

QE (%)
       (1230 nm)
       (2000 nm)
	>50
	>50
			72
			82	

LINEAR RANGE (e-)	>60,000	95,000 (100kHz) 101,000 (1MHz)	92,000 (100kHz) >100,000 (1MHz)	87,000 (100kHz) 100,000 (1MHz)
OPERABILITY (%)	>95 (at 36 μm)	>99,5	>99,5	

Table 6. Summary of 36-μm pixels FPA performances.

Performance parameter	Requirements	Measured (125K)	Measured (132K)	Measured (144K)
RON (100kHz) **(e-) (1MHz)**	<40 <80		39 68	
GAIN (100kHz) **(e-/DN) (1MHz)**			2.16 33.56	
DARK (e-/s)	<5,000		<30	
LINEAR RANGE (e-)	>240,000	380,000 (100kHz) 404,000 (1MHz)	368,000 (100kHz) >400,000 (1MHz)	348,000 (100kHz) 400,000 (1MHz)
OPERABILITY (%)	>95	>99	>99	

6. CONCLUSION

The tests performed during this campaign allowed for the assessment of the performances of the VIS-NIR MAJIS flight detector through the characterization of the parameters described in Section IV.
The results obtained from the analysis of these tests show that the detector:

● follow closely the noise model,
● has RONs within operability requirements and in agreement with our expectations,
● the linear behavior remains within 2% for the large majority of the dynamic range,
● the quantum efficiency varies between 0.72 and 0.92 for a requirement of 0.5,
● the operability is completely satisfying (> 99%).

Although some measurements could not be performed in nominal conditions the analysis of the tests showed that the VIS-NIR FPA fills the requirements which were derived based on the scientific goals of MAJIS.

REFERENCES

[1] Carter, J., et. al. "MAJIS IR Channel: 3) Performance of the Focal Plane Unit" Proc. SPIE this conference, (2022).
[2] Langevin, Y., et. al. "H1RG readout procedures for MAJIS, the VIS/NIR imaging spectrometer of JUICE: impacts on the performances" Proc. SPIE this conference, (2022).
[3] Bolsée, D., et. al. "Characterization facility for the MAJIS/JUICE VIS-NIR FM and SM detectors." Space Telescopes and Instrumentation 2020: Optical, Infrared, and Millimeter Wave (Vol. 11443, pp. 1214-1233). SPIE, (2020, December).
[4] Cisneros-González, M. E., et. al. "MAJIS/JUICE VIS-NIR FM and SM detectors characterization." Space Telescopes and Instrumentation 2020: Optical, Infrared, and Millimeter Wave (Vol. 11443, pp. 271-285). SPIE, (2020, December).
[5] Seshadri, S., Cole, D. M., Hancock, B. R., & Smith, R. M. "Mapping electrical crosstalk in pixelated sensor arrays." High Energy, Optical, and Infrared Detectors for Astronomy III (Vol. 7021, pp. 54-64). SPIE, (2008, July).